Supporting Information

An anionic metal–organic framework: metathesis of Zinc(II) with Copper(II) for efficient C_3/C_2 hydrocarbon and organic dyes separation

Xiuping Liu, Chunlian Hao, Jing Li, Yutong Wang, Yongchun Hou, Xue Li, Lianming Zhao*, Houyu Zhu, Wenyue Guo*

College of Science, China University of Petroleum, Qingdao, Shandong 266580, People's Republic of China.

E-mail: lmzhao@upc.edu.cn; wyguo@ upc.edu.cn.

Tel: +86-532-8698-3363; Fax: +86-532-8698-3363.

Contents

S1. General experimental chemicals and methods

S2. Synthesis of NEM-7-Zn

S3. Crystal data of complex NEM-7-Zn

S4. Determination of single-crystal structure

S5. A typical procedure for the dye adsorption experiments

S6. The TG curve of NEM-7-Zn

S7. IR spectra

S8. Powder X-ray diffraction of NEM-7-Zn and NEM-7-Cu

S9. Metal metathesis of Zn to Cu

S10. The adsorption properties in NEM-7-Cu

S11. The dye adsorption in NEM-7-Cu

S1. General experimental chemicals and methods

All chemical reagents were used as commercially obtained without further purification except H_5**N**. The ligand H_5**N** was prepared according to the ref. 20. X-ray powder diffractions were measured on a Panalytical X-Pert pro diffractometer with Cu-Kα radiation. Infrared spectra were recorded on a Bruker VERTEX-70 spectrometer as KBr pellets in the frequency range 4000-400 cm^{-1}. The elemental analyses (C, H, and N) were determined on a CE instruments EA 1110 analyzer. Low pressure (< 800 torr) gas (N_2, CO_2 and CH_4) sorption isotherms were measured using a Micrometrics ASAP 2020 surface area and pore size analyzer. TG curves were measured from 40 to 900 °C on a Mettler Toledo TGA instrument at a heating rate 10 °C/min under the N_2 atmosphere (100 ml min^{-1}). Inductively coupled plasma optical emission spectrometer (ICP-OES) measurements were carried out on Optima 5300 DV.

S2. Synthesis of NEM-7-Zn

A mixture of $Zn(NO_3)_2 \cdot 3H_2O$ (10 mg) and H_5**N** (2 mg) was dissolved in 4 ml DMF mixed solvent, and then 0.1 ml HNO_3 was added. All the reagents were sealed in a glass bottle and slowly heated to 90°C from room temperature in 6 h. After keeping at 90°C for 50 h, the mixture was slowly cooled to 30°C at a rate of 7°C/h. The creamy white block crystals could be collected after washed with DMF and dried in the air. The sample of NEM-7-Zn in 65% yield based on zinc was insoluble in common solvent, such as H_2O, dichloromethane, methanol, DMSO.

S3. Crystal data of complex NEM-7-Zn

Table S1 Crystal data and structure refinement for complex NEM-7-Zn

Parameters of crystal structure	Values
Formula	$C_{30}Zn_2O_{11}H_{31}N_4$
M	754.33
Crystal system	orthorhombic
Space group	*P2bc2*
a/Å	13.4950(6)
b/Å	13.7761(5)
c/Å	26.8721(8)
α/deg	90.0
β/deg	90.0
γ/deg	90.0
V/Å^3	4995.83(3)
Z	4
GOF	1.050
R_1^a/wR_2^b $I > 2\sigma(I)$	0.0501,0.2073
R_1, wR_2 (all data)	0.0325,0.2003
R_{int}	0.0383

$^aR_1 = \Sigma||F_o| - |F_c||/\Sigma|F_o|$. $^bwR_2 = [\Sigma w(F_o^2 - F_c^2)^2/\Sigma w(F_o^2)^2]^{0.5}$.

S4. Determination of single-crystal structure

Single crystal of the prepared complex with appropriate dimensions was chosen under an optical microscope and quickly coated with high vacuum grease (Dow Corning Corporation) before being mounted on a glass fiber for data collection. Data for NEM-7-Zn were collected on Super Nova diffractometer equipped with a Cu-K_α radiation X-ray sources (λ = 1.54 Å) and an Eos CCD detector under 100 K. For NEM-7-Zn, data were measured using scans of 0.5° per frame for 10 s until a complete hemisphere had been collected. Data reduction was performed with the CrysAlisPro package, and an analytical absorption correction was performed. The structures were treated anisotropically, whereas the aromatic and hydroxy-hydrogen atoms were placed in calculated ideal positions and refined as riding on their respective carbon or oxygen atoms. We employed PLATON[1] and SQUEEZE[2] to calculate the diffraction contribution of the solvent molecules and thereby produced a set of partly solvent-free diffraction intensities.

S5. A typical procedure for the dye adsorption experiments

In the adsorption process, the adsorbent NEM-7-Cu (5 mg) was weighed precisely and immersed in CH_3OH solutions (5 ml) containing dye molecules (concentration: 4×10^{-5} mol l^{-1}), such as methylene blue (MB^+), crystal violet (CV^+), rhodamine B (RB^+), methyl orange (MO^-), and Sudan II (SD^0). Then the UV-Vis spectra of CH_3OH solutions containing both dyes and adsorbent were measured at 25°C at different time points (10 min to 12 h) to calculate the dye concentrations by comparing the UV-Vis absorbance of the dye and adsorbent containing solutions at various time to that of the original dye containing solution.

S6. The TG curve of NEM-7-Zn and NEM-7-Cu

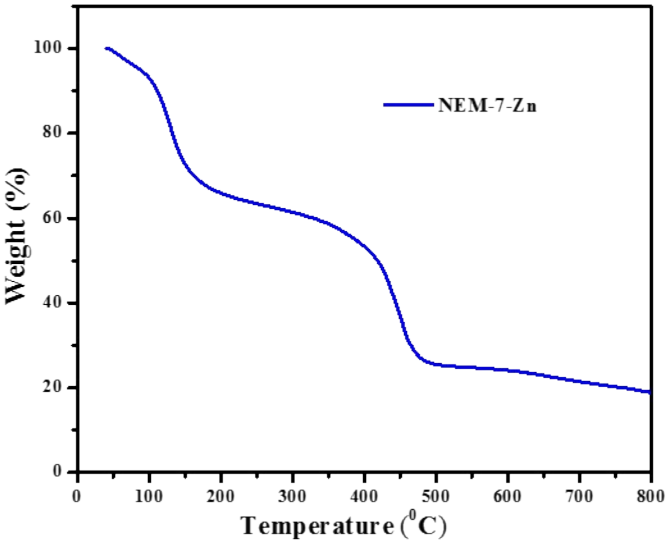

Fig. S1 TG curve of NEM-7-Zn.

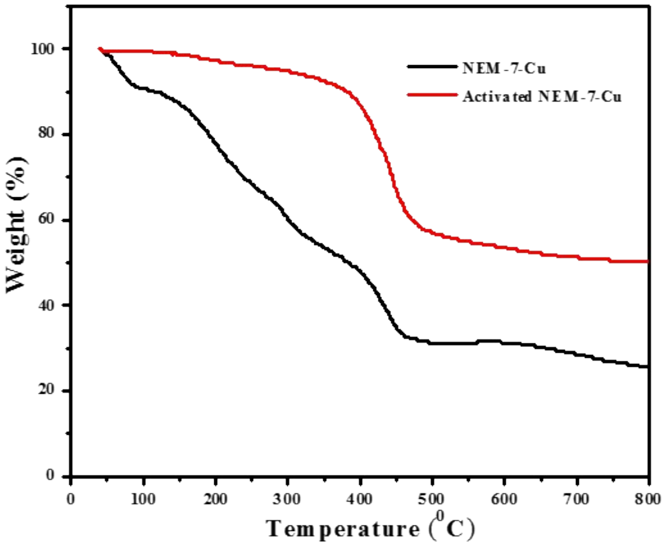

Fig. S2 TG curve of NEM-7-Cu before and after activation.

S7. IR spectra

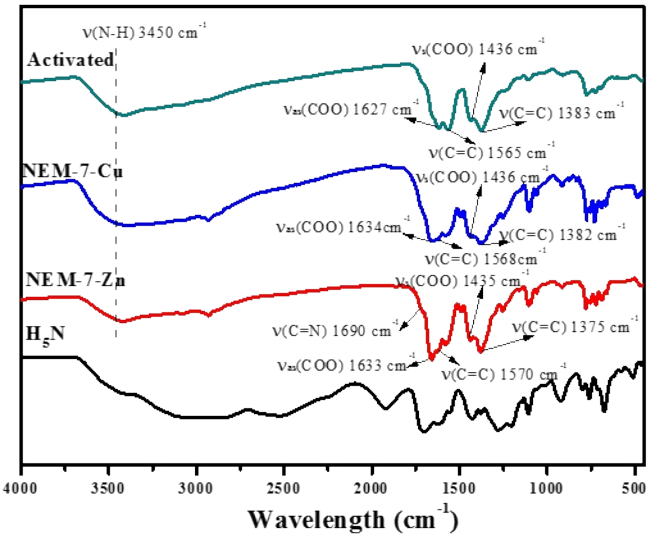

Fig. S3 FT-IR spectra of ligand H_5**N**, NEM-7-Zn and NEM-7-Cu in the as-synthesized, and activated adsorbed states.

S8. Powder X-ray diffraction of NEM-7-Zn

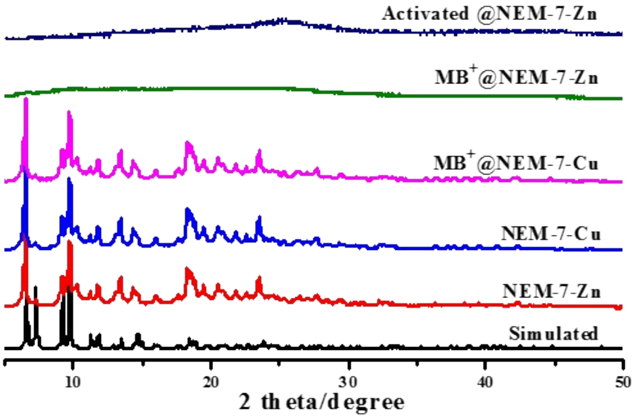

Fig. S4 XRD patterns of NEM-7-Zn simulated from X-ray crystal diffraction data (black) and measured for NEM-7-Zn (red) and NEM-7-Cu (blue) samples in the as-synthesized, fully MB^+ adsorbed states of NEM-7-Zn (purple) and NEM-7-Cu (green), activated states (navy) of NEM-7-Zn, respectively.

S9. Metal metathesis of Zn to Cu

1. ICP results

Table S2 ICP results of the compounds treated by metal metathesis on NEM-7-Zn after six days

Sample	Solvent	Cu Content (wt %)	Zn Content (wt %)
NEM-7-Zn	DMF	4.60	11.06
NEM-7-Zn	DMF:CH_3OH (1:1)	8.72	7.87
NEM-7-Cu	DMF:CH_3OH (1:3)	15.38	0.42
NEM-7-Cu	CH_3OH	15.66	0.20

2. Elemental EDX mapping

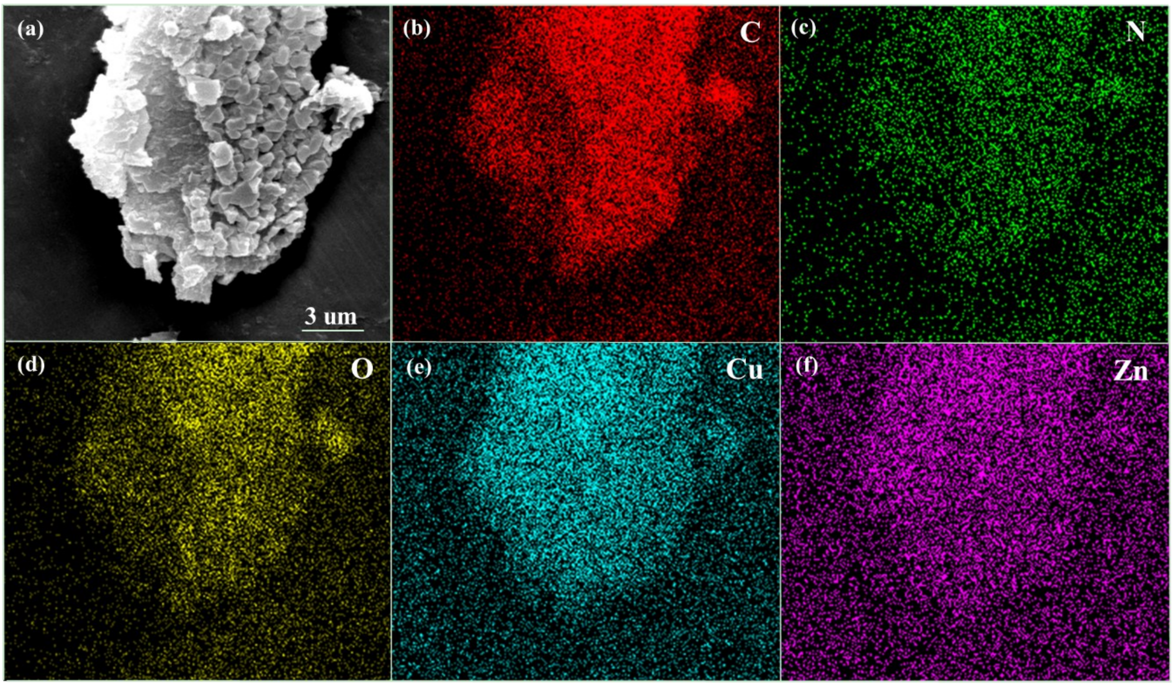

Fig. S5 Morphology of the crystals on the halfway of Zn to Cu transformation. (a) SEM image; (b-f) C, N, O, Cu, and Zn elemental EDX mapping.

S10. The adsorption properties in NEM-7-Cu

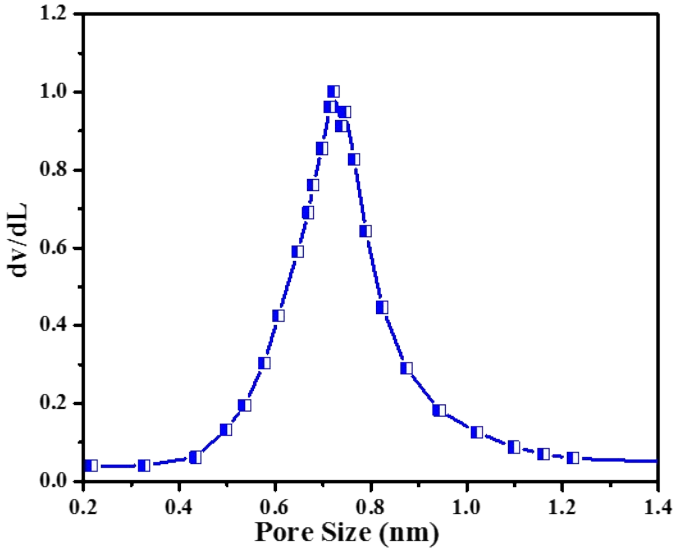

Fig. S6 Pore size distribution for NEM-7-Cu evaluated by using N_2 adsorption data measured at 77 K.

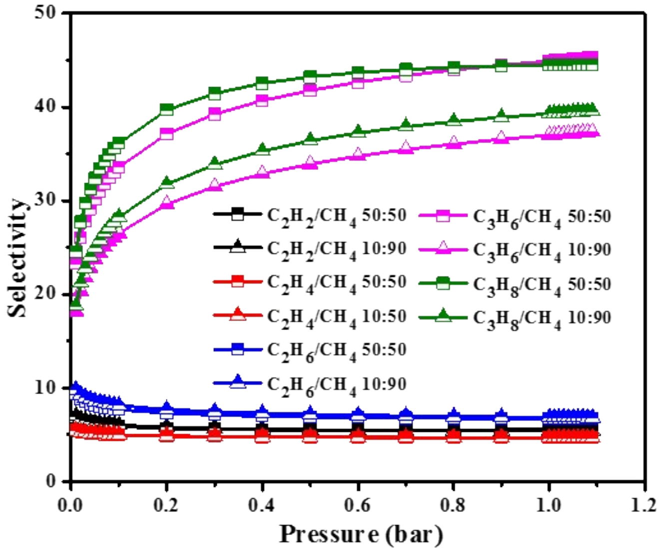

Fig. S7 Adsorption selectivities of NEM-7-Cu calculated by the IAST method for mixtures of C_2H_2/CH_4, C_2H_4/CH_4, C_2H_6/CH_4, C_3H_6/CH_4, and C_3H_8/CH_4 at 298 K.

Table S3 Adsorption selectivity of hydrocarbon at 298 K for the molar ratio at 50:50 binary mixtures

	Pore size [Å]	IAST selectivity									Ref.
		C_3H_6 /C_2H_2	C_3H_6 /C_2H_4	C_3H_8 /C_2H_2	C_3H_8 /C_2H_4	C_2H_2 /CH_4	C_2H_4 /CH_4	C_2H_6 /CH_4	C_3H_6 /CH_4	C_3H_8 /CH_4	
NEM-7-Cu[a]	7	6.8	8.6	7.1	8.82	7.1	5.5	9.4	44.6	45.3	This work
UPC-33[a]	4.3	3.8	5.7	3.78	5.66	7.7	4.48	4.8	42.4	41.7	3
FJI-C1[a]	7.8			4.1		9.7	6.6	9.0		471	4
NEM-4[b]	10-21	5.2	6.8	5	6.6	63.4	44.3	20.1	174	168	5, This work
UPC-21	14-27					38.1	23.5	15.3	75	67	6
LIFM-38[a]	9.6		6.4		6.7		6.5	8.2	34.4	35.8	7
ZnSDB[a]	4.7-5					16.9	15.9	23.2			8
MFM-202a[c]	9		9			12	8	10.2	105	75	9
UTSA-35a[a]	5-11					24	10	15	132	130	10
FJI-C3[a]	5-7					14.6	23.7	39.9			11
FJI-C5[a]	5-8					14.5	19.0	33.3			11

[a] at 298 K and 1 bar. [b] at 295 K and 1 bar. [c] at 293 K and 1 bar.

Table S4 Summary of physical parameters of light hydrocarbons[6]

gas	Kinetic diameter (Å)	Critical temp (°C)	Dipole moment (10^{-30} C m)	Quadrupole moment (10^{-40} C m^2)	Polarizability (10^{-25} cm^3)	Molecular radius (Å)
CH_4	3.758	-82.60	0	0	25.93	2.276
C_2H_2	3.3	35.75	0	-	33.3-39.3	-
C_2H_4	4.163	9.2	0	5.00	42.52	-
C_2H_6	4.4443	32.17	0	2.17	44.3-44.7	2.655
C_3H_6	4.678	91.06	1.22	-	62.6	-
C_3H_8	4.3-5.118	96.7	0.28	-	62.9-63.7	2.946

S11. The dye adsorption in NEM-7-Cu

Based on the stable nanotubular channels of charged NEM-7-Cu, we explored its potential application in dye capture by host-guest electrostatic interactions and/or guest-guest exchange interactions. Generally, the size and charged state of large dye molecules in solution are the two most important factors in the dye adsorption and separation process. Thus, we carefully selected five dyes molecules with different shapes/sizes and charge to study the properties for dye capture, including anionic dye Methyl orange (MO^-), neutral dye Sudan II (SD^0), as well as cationic dyes MB^+, Crystal violet (CV^+), and Rhodamine B (RB^+).

First, NEM-7-Cu was examined to determine the uptakes of dye molecules with different charged states (Fig. S6), i.e., MB^+, SD^0, and MO^- in their CH_3OH solutions (5 mL, 4×10^{-5} M). Compared with other reported MOFs for dye sorption, NEM-7-Cu does not need any activation process. The content of dye in the solution was detected at certain time intervals through UV-Vis spectroscopy. As shown in Fig. 5a, the absorption peak value of the MB^+ solution is gradually decreased, and then nearly all the MB^+ are absorbed up to 12 h by NEM-7-Cu. However, the absorption peak of neutral dyes SD^0 decreases slightly, and the anionic MO^- dyes absorption peak retains even after 12 h (Fig. S7). Correspondingly, the color of MB^+ solution fades to colorless after the addition of NEM-7-Cu, whereas it retains for the SD^0 and MO^- containing solutions even after 12 h (Fig. S9). To further demonstrate the selective adsorption of cationic dye, the separation performance of NEM-7-Cu in (1:1) mixtures of MB^+/SD^0 and MB^+/MO^- solutions were studied. As shown in Fig. 5b,c, NEM-7-Cu could selectively absorb MB^+, while MO^- and SD^0 remain in the CH_3OH solutions even after 12 h. The colors of the mixed MB^+/MO^- and MB^+/SD^0 solutions change significantly and at last are almost identical to those of the pure MO^- and SD^0 solutions, respectively (Fig. S10c,d). Therefore, NEM-7-Cu could be used to selectively separate organic dyes with similar sizes but different charges utilizing ion-exchange processes.

To further verify that the selective absorption toward cationic dyes via the ion exchange process, dye releasing experiments were also carried out in the NaCl-containing methanol solution and pure methanol solution, respectively. As shown in Fig. 5b, the MB^+ molecules loaded in NEM-7-Cu can be efficiently released in NaCl-containing solution. The release reaches a plateau at 70 min, and after 90 min the release efficiency is up to 42.1%. However, only a trace amount of MB^+ is released in CH_3OH solution. Therefore, the release of MB^+ in NaCl-containing solution is triggered by Na^+ cations. These results further confirm that an ion-exchange process occurred between MB^+ in NEM-7-Cu and Na^+ in NaCl-containing methanol solution.

Furthermore, the adsorption ability of NEM-7-Cu toward dyes with different sizes/shape was also examined. The size of three positive organic dyes follows the order $MB^+ < CV^+ < RB^+$ (Fig. S6 and Table S4). In contrast to the good adsorption performance for MB^+ (Fig. 5a) as mentioned above, NEM-7-Cu is indeed unable to adsorb RB^+ or weakly capture CV^+ from the methanol solution (5 mL, 4×10^{-5} M), mirrored by the variation of the dye concentrations induced by NEM-7-Cu (Fig. S7a,b), suggesting that molecular size is an important factor for dye to be captured by NEM-7-Cu. As shown in Fig. S8a, the adsorption rate of dye molecules follows the sequence $MB^+ > CV^+ > RB^+$, correlating with the sequence of the molecular sizes. After 12 h, only 19% MB^+ concentration can be detected in the solution, while the values for CV^+ and RB^+ are 69.2% and 99%, respectively, suggesting NEM-7-Cu has a high MB^+ capture and separation efficiency. The large size of RB^+ might be a main factor of hindering to be absorbed by NEM-7-Cu. To further confirm whether NEM-7-Cu can be employed to separate dye molecules with different size, samples was immersed in the 1:1 mixed MB^+/RB^+ and CV^+/MB^+ solutions, and UV-Vis spectra were utilized to evaluate the separation capability of NEM-7-Cu. As shown in Fig. 6e-f, the UV-Vis spectra indicate that the absorption peak of MB^+ at around 665 nm decreases quickly with time, whereas it decreases relatively slowly for CV^+ or does not change for RB^+ even after 12 h. Correspondingly, the colors are also rapidly changed with the time (Fig. S10a,b). These facts suggest that the molecular size is of significant importance for the dye adsorption.

NEM-7-Cu (50 mg) was also used to filter MB^+ from its CH_3OH solution at different filter amounts (0-16 mL) (Fig. S8b and Fig. S11). Compared with the original solution, the large loss of MB^+ concentration in the outflow indicates the successful removal of MB^+ from the CH_3OH solution (Fig. 5d). We can find that NEM-7-Cu maintains a filter efficiency of 100% even at 120 mL g^{-1}, indicating it is one of the highest filter efficiency for MB^+.[12] After that, the filter efficiency slowly drops due to the penetration of dye molecules. When the amount of solution reaches 16 mL (320 mL g^{-1}), the filter efficiency remains 67%.

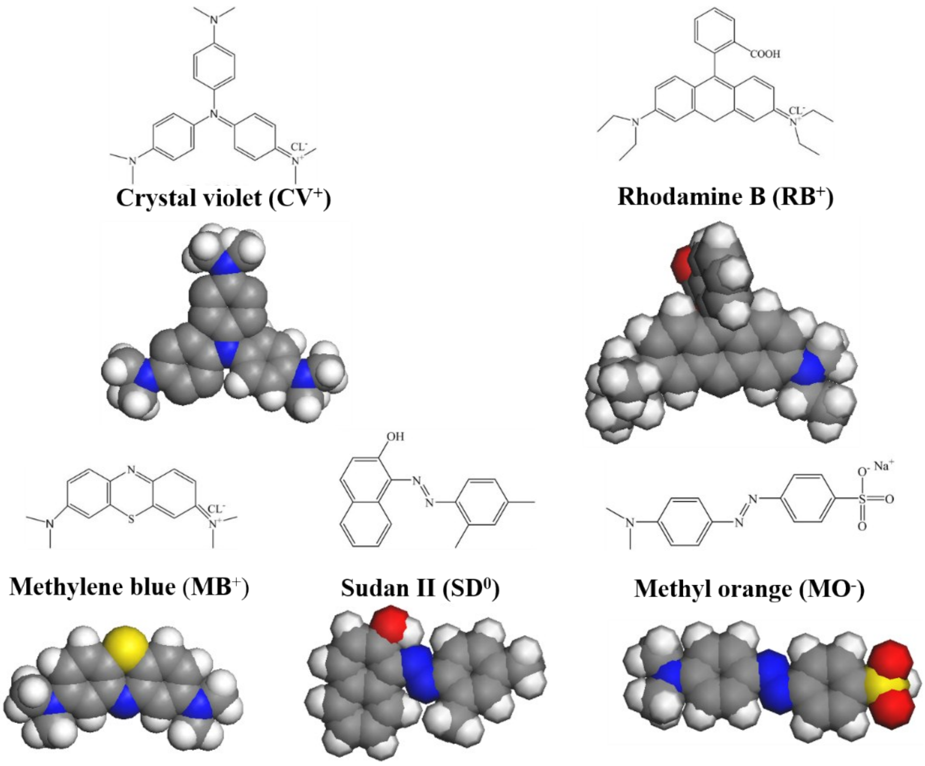

Crystal violet (CV+)

Rhodamine B (RB+)

Methylene blue (MB+)

Sudan II (SD0)

Methyl orange (MO-)

Fig. S8 The structural formula of the studied dye molecules.

Table S5 Molecular dimensions of dye molecules with different charges

	MB^+	CV^+	RB^+	SD^0	MO^-
a (Å)	2.62	4.78	6.53	3.88	4.14
b (Å)	5.94	12.42	11.89	7.21	5.65
c (Å)	14.61	13.10	15.55	11.06	13.65

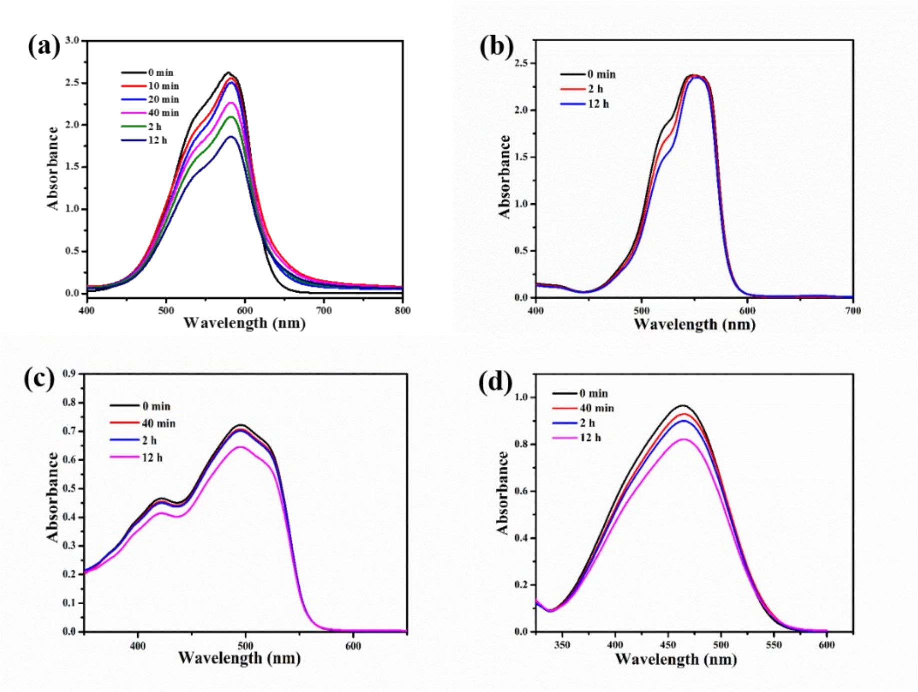

Fig. S9 UV-Vis spectra of the CH_3OH solutions containing (a) CV^+, (b) RB^+, (c) SD^0, and (d) MO^- at different time points in an adsorption test with NEM-7-Cu.

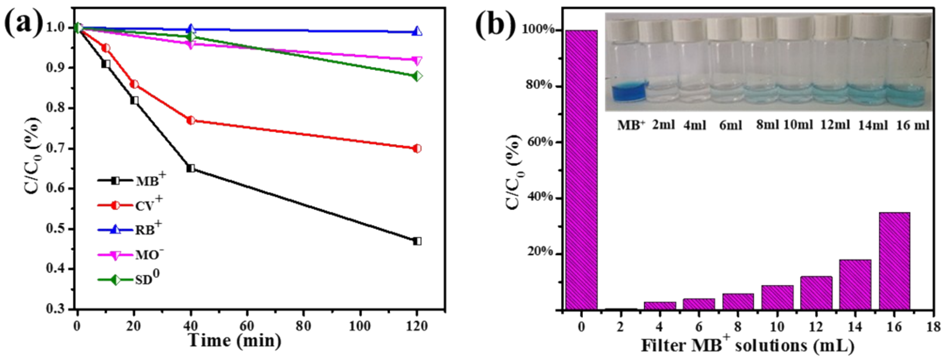

Fig. S10 (a) Concentration changes of MB$^+$, CV$^+$, RB$^+$, MO$^-$, and SD^0 in CH_3OH solution with time induced by NEM-7-Cu. (b) Filtrates collected at different filter amounts of MB$^+$ in CH_3OH solution as well as the corresponding concentrations of MB$^+$, the amount of the adsorbent was 50 mg.

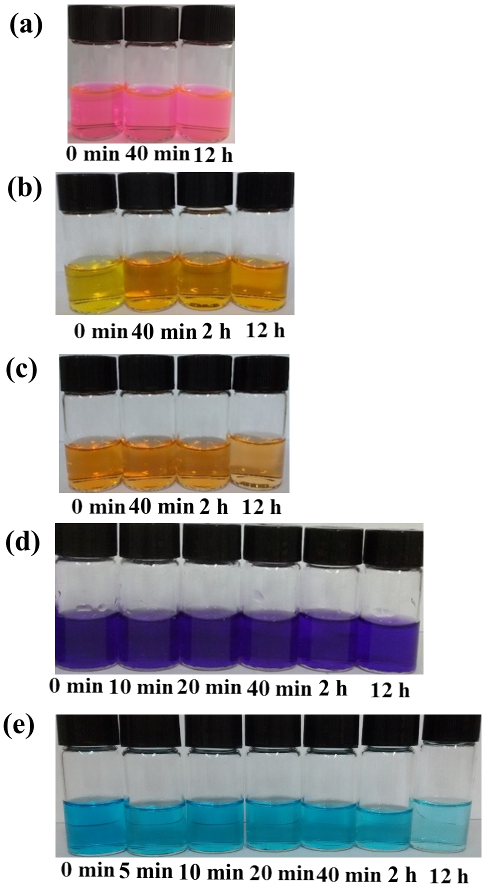

Fig. S11 Photographs of the CH_3OH solutions containing (a) RB^+, (b) SD^0, (c) MO^-, (d) CV^+, and (e) MB^+ at different time points in an adsorption test with NEM-7-Cu.

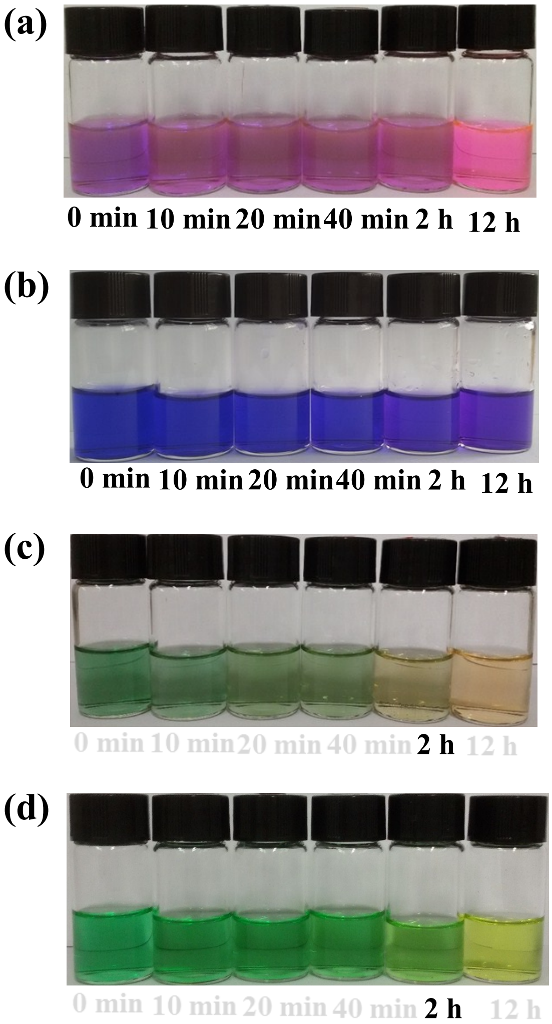

Fig. S12 Photographs of the CH_3OH solutions containing (a) MB^+/RB^+ (1:1), (b) MB^+/CV^+ (1:1), (c) MB^+/SD^0 (1:1), and (d) MB^+/MO^- (1:1) dye mixtures at different time points in an adsorption test with NEM-7-Cu.

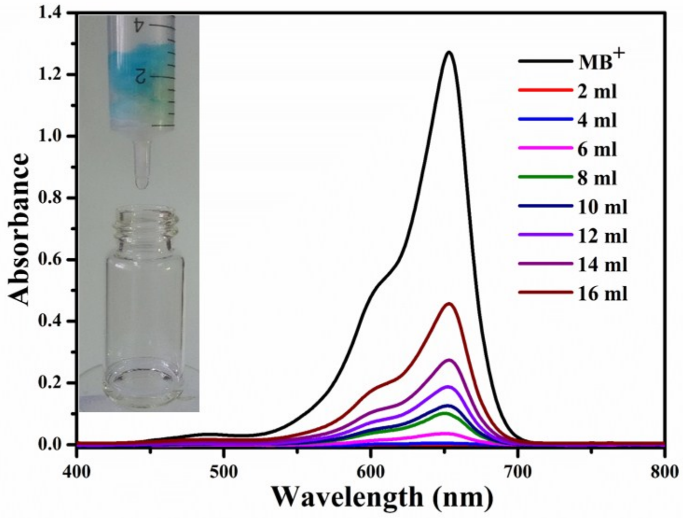

Fig. S13 UV-Vis spectra of different filter amounts of MB^+ in CH_3OH solution. The insert shows a photograph taken in the filter process.

References

1 L. Sarkisov, A. Harrision, *Mol. Simul.*, 2011, **37**, 1248–1257.

2 A. L. Spek, *J. AppCryst.*, 2003, **36** 7–13.

3 W. D. Fan, Y. T. Wang, Q. Zhang, A. Kirchon, Z. Xiao, L. Zhang, F. Dai, R. Wang, D. F. Sun, *Chemistry*, 2018, **24***,* 2137−2143.

4 Y. Huang, Z. Lin, H. Fu, F. Wang, M. Shen, X. Wang, R. Cao, *ChemSusChem.*, 2014, **7**, 2647–2653.

5 X. P. Liu, W. D. Fan, M. H. Zhang, G. X. Li, H. J. Liu, D. F. Sun, L. M. Zhao, H. Y. Zhu, W. Y. Guo, *Mater. Chem. Front.*, 2018, **2**, 1146–1154.

6 M. H. Zhang, X. L. Xin, Z. Y. Xiao, R. M. Wang, L. L. Zhang, D. F. Sun, *J. Mater. Chem. A,* 2017, **5**, 1168–1175.

7 C. X. Chen, Z. W. Wei, Q. F. Qiu, Y. Z. Fan, C. C. Cao, H. P. Wang, J. J. Jiang, D. Fenske, C. Y. Su, *Crys. Growth Des.*, 2017, **17***,* 1476–1479.

8 F. S. Tang, R. B. Lin, R. G. Lin, J. C. G. Zhao, B. Chen, *J. Sol. State Chem.*, 2018, **258**, 346–350.

9 S. Gao, C. G. Morris, Z. Lu, Y. Yan, H. G. W. Godfrey, C. Murray, C. C. Tang, K. M. Thomas, S. Yang, M. Schröder, *Chem. Mat.*, 2016, **28** 2331–2340.

10 Y. He, Z. Zhang, S. Xiang, F. R. Fronczek, R. Krishna, B. Chen, *Chem. Commun.*, 2012, **48**, 6493–6495.

11 L. Li, Q. Yin, H. F. Li, T. F. Liu, R. Cao, *Mater. Chem. Front.*, 2018, **2**, 1436–1440.

12 M. L. Ma, J. H. Qin, C. Ji, H. Xu, R. Wang, B. J. Li, S. Q. Zang, H. W. Hou, S. R. Batten, *J. Mater. Chem. C.*, 2014, ***2***, 1085–1093.